Artificial Cells, Nanomedicine, and Biotechnology
An International Journal

ISSN: (Print) (Online) Journal homepage: https://www.tandfonline.com/loi/ianb20

Intracellular synthesis of gold nanoparticles by *Gluconacetobacter liquefaciens* for delivery of peptide CopA3 and ginsenoside and anti-inflammatory effect on lipopolysaccharide-activated macrophages

Ying Liu, Haribalan Perumalsamy, Chang Ho Kang, Seung Hyun Kim, Jae-Sam Hwang, Sung-Cheol Koh, Tae-Hoo Yi & Yeon-Ju Kim

To cite this article: Ying Liu, Haribalan Perumalsamy, Chang Ho Kang, Seung Hyun Kim, Jae-Sam Hwang, Sung-Cheol Koh, Tae-Hoo Yi & Yeon-Ju Kim (2020) Intracellular synthesis of gold nanoparticles by *Gluconacetobacter liquefaciens* for delivery of peptide CopA3 and ginsenoside and anti-inflammatory effect on lipopolysaccharide-activated macrophages, Artificial Cells, Nanomedicine, and Biotechnology, 48:1, 777-788, DOI: 10.1080/21691401.2020.1748639

To link to this article: https://doi.org/10.1080/21691401.2020.1748639

ARTIFICIAL CELLS, NANOMEDICINE, AND BIOTECHNOLOGY
2020, VOL. 48, NO. 1, 777–788
https://doi.org/10.1080/21691401.2020.1748639

Intracellular synthesis of gold nanoparticles by *Gluconacetobacter liquefaciens* for delivery of peptide CopA3 and ginsenoside and anti-inflammatory effect on lipopolysaccharide-activated macrophages

Ying Liu[a], Haribalan Perumalsamy[a], Chang Ho Kang[b], Seung Hyun Kim[a], Jae-Sam Hwang[c], Sung-Cheol Koh[d], Tae-Hoo Yi[a,b] and Yeon-Ju Kim[a,b]

[a]Graduate School of Biotechnology and College of Life Science, Kyung Hee University, Gyeonggi-do, Republic of Korea; [b]Division of Applied Life Science and PMBBRC, Gyeongsang National University, Jinju, Republic of Korea; [c]Department of Agricultural Biology, National Institute of Agricultural Sciences, Rural Development, Wanju, Republic of Korea; [d]Department of Environmental Engineering, Korea Maritime and Ocean University, Busan, Republic of Korea

ABSTRACT

Probiotic Gluconacetobacter strains are intestinal microbes with beneficial effects on human health. Recently, researchers have used these strains to biosynthesize metal and non-metal nanoparticles for treating various chronic diseases. Despite their importance in nanotechnology, gold nanoparticles (AuNPs) biosynthesized by Gluconacetobacter species have not been clearly identified for treating inflammation and inflammation-associated diseases. While ginsenoside CK has strong pharmaceutical activity, it also has strong cytotoxicity and hydrophobicity which is hurdle to make formulation. Peptide–nanoparticle hybrids are gaining increasing attention for their potential biomedical applications, including human inflammatory diseases. Herein, we developed peptide CopA3 surface conjugated and ginsenoside compound K (CK) loaded gold nanoparticles (GNP-CK-CopA3), which intracellularly synthesised by the probiotic *Gluconacetobacter liquefaciens* kh-1, to target lipopolysaccharide (LPS)-activated RAW264.7 macrophages. The synthetic GNP-CK-CopA3 was characterised by various instrumental techniques. The results of our cellular uptake and MTT assays exhibited obvious drug intracellular delivery without significant cytotoxicity. In addition, pre-treatment with GNP-CK-CopA3 significantly ameliorated LPS-induced nitric oxide (NO) and reactive oxygen species (ROS) production and suppressed the mRNA and protein expression of pro-inflammatory cytokines in macrophages. Furthermore, GNP-CK-CopA3 efficiently inhibited the activation of the nuclear factor-κB (NF-κB) and mitogen-activating protein kinase (MAPK) signalling pathways. Taken together, our findings highlight the potential of using peptide–nanoparticle hybrids in the development of anti-inflammatory approaches and providing the experimental foundation for further application.

GRAPHICAL ABSTRACT

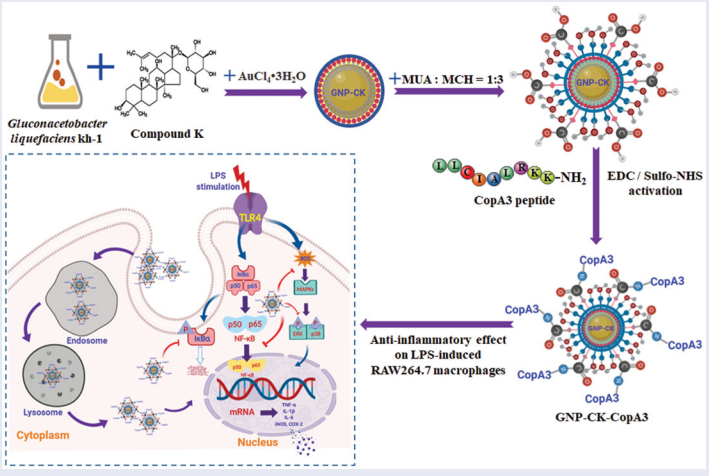

ARTICLE HISTORY

Received 8 October 2019
Revised 14 February 2020
Accepted 24 February 2020

KEYWORDS

Peptide CopA3; Compound K; gold nanoparticles; anti-inflammatory; NF-κB

CONTACT Yeon-Ju Kim yeonjukim@khu.ac.kr; Tae-Hoo Yi drhoo@khu.ac Graduate School of Biotechnology and College of Life Science, Kyung Hee University, Gyeonggi-do, Republic of Korea

Supplemental data for this article is available online at https://doi.org/10.1080/21691401.2020.1748639.

Introduction

Panax ginseng Meyer, a perennial plant of the Araliaceae family, is one of the most well-known herbal medicines and has been used in Eastern countries for more than two thousand years. Ginseng exhibits various pharmacological effects including, anti-cancer, anit-diabetes, anti-inflamaroty, anti-oxidanat, stimulation of immune system, and nervous system, hyperglycaemia, and cardiovascular diseases [1–4]. Ginsenoside compound K (CK) is a major intestinal bacterial metabolite of the protopanaxadiol-type ginsenosides. CK has attracted wide attention because of its multiple pharmacological actions, such as anti-cancer, anti-inflammatory, anti-aging, and anti-diabetic effects [5,6]. However, its clinical application is significantly restricted by its low water solubility and poor permeability [7]. To overcome those issues, various nanotechnology-based systems have been developed to improve drug delivery and thereby overcome low therapeutic effectiveness [8]. Inflammation is the major response raised by the body to address injuries. Despite inflammation establishing a vital constituent of tissue repair, it is well recognised that unrestrained or chronic inflammation becomes deleterious, leading to progressive tissue damage. This complex, tightly regulated process serves as a rapid defence mechanism to contain potential pathogens, limit further tissue damage, and stimulate repair mechanisms; consequently, inflammation is crucial for human health [9]. Ginsenoside CK is well-known for its anti-inflammatory effects in lipopolysaccharide (LPS)-activated RAW 264.7 cells [4], LPS-induced septic mouse brains [10], and 2,4,6-trinitrobenzene sulphuric acid–induced colitic mice [11]. Its underlying mechanisms include inhibition of activation of nuclear factor NF-κB and mitogen-activated protein kinases [10,11].

The potential applications of gold nanoparticles (GNPs) in diagnosis, therapy, and drug delivery have been extensively studied [8]. Various chemical, physical, and electrochemical technologies have been developed to generate GNPs. However, the toxic reagents limited the biomedical applications of nanoparticles [12]. So recently, many researchers, including our group, have focussed on the biological synthesis of GNPs to allow easy synthesis, biocompatibility, distinctive physicochemical properties, and other benefits [13]. Microorganisms can be used for the synthesis of GNPs because of their considerable ability to reduce metal ions without producing any toxic by-products [14,15]. Previous studies showed that *Lactobacillus* strains can be used to extracellularly or intracellularly biosynthesize GNPs [15,16]. Herein, we synthesised GNPs using probiotic *Gluconacetobacter liquefaciens* kh-1 (family *Acetobacteraceae*) for CK loading.

Previous investigations have shown that GNPs are readily bound thiol, amine, and cyanide groups [17]. GNPs have been further functionalised with different complex molecules, including DNA [18], proteins [19], peptides [20], and polymers [21]. Antimicrobial peptides have received considerable interest due to their activity against multi-drug-resistant microbes and antitumor functions [22]. CopA3 is a 9-mer peptide (LLCIALRKK-NH_2) derived from an insect defensin peptide, coprisin, produced by *Copris tripartitus* [23]. It has been reported to exert antibacterial effects against various pathogenic bacteria [24] and selective anticancer on human gastric cancer cells [25]. CopA3 also ameliorated inflammatory responses in the gut [26] and lipopolysaccharide (LPS)-induced macrophage activation [27].

Herein, CK and CopA3 have been loaded and bioconjugated on GNPs and then evaluated its anti-inflammation in LPS-induced RAW264.7 macrophages.

Materials and methods

Materials

MRS (de Man, Rogosa, and Sharpe) broth and agar were purchased from MB Cell (Seoul, Republic of Korea). Dulbecco's modified Eagle's medium (DMEM), foetal bovine serum (FBS), and penicillin-streptomycin were all obtained from GenDEPOT (Barker, TX). Gold(III) chloride trihydrate ($HAuCl_4{\cdot}3H_2O$), 3-(4,5-dimethylthiazol-2-yl)-2,5-diphenyltetrazolium bromide (MTT), dimethyl sulfoxide (DMSO), lipopolysaccharide (LPS, *Escherichia coli* 011: B4), and all other chemicals used herein were purchased from Sigma-Aldrich Chemicals (St. Louis, MO, USA). All methods followed the relevant guidelines and regulations.

Analysis of nanoparticle-producing strain and growth condition evaluation

Strain kh-1 was kindly provided by Seung-Cheol Koh (Professor, Korea Maritime University) and cultured on a solid nutrient medium containing 5 g/L yeast extract, 3 g/L peptone, 25 g/L mannitol, and 15 g/L agar at 30 °C for 48 h. The colonies were picked from agar plates and suspended in a modified YPM medium containing 5 g/L yeast extract, 3 g/L peptone, 25 g/L mannitol, and 15 g/L agar. All culture media were sterilised at 121 °C for 15 min. The phylogenetic tree showed in Supplementary Figure 1, was constructed following our previous method [11], and the identified 16S ribosomal RNA sequences were deposited in NCBI GenBank under accession No. MN209894.

Intracellular synthesis of GNP-CK

The ginsenoside CK–loaded GNPs were synthesised according to our previously published with few modifications [16]. *G. liquefaciens* kh-1 was cultivated in MRS broth at 27 °C for 24 h, and the activated culture was inoculated into MRS broth at 27 °C on a shaker bed at 200 rpm for 24 h. After incubation, the fresh biomass was collected by centrifuging at 3,000 rpm for 10 min at 4 °C. The collected bacterial pellets were washed and resuspended in the sterile water (10 ml). The gold chloride trihydrate solution ($HAuCl_4{\cdot}3H_2O$, final concentration of 1 mM) and CK (final concentration of 1.6 mM) were inoculated with *G. liquefaciens* and incubated at 27 °C in a shaker bed for 24 h. Afterward, the synthetic of GNPs was visually observed according to the colour change. The mixtures were conducted ultra-sonication in ice for 30 min to release GNPs and then centrifuged at 3000 rpm for 10 min to

remove the bacterial pellets. Finally, the CK-loaded nanoparticles (GNP-CK) were collected by high-speed centrifugation (12,000 rpm for 10 min at 4 °C), washed exhaustively and resuspended in sterile water.

Conjugation of GNP-CK with peptide CopA3

To conjugate the peptide CopA3, a carboxylic acid-terminated alkanethiol monolayer was first formed on the surface of the nanoparticles, as previously reported [28]. Afterward, 100 μM CopA3 (dissolved in phosphate-buffered saline, PBS) was added to the 1-ethyl-3-(3-dimethylamino-propyl)carbodiimide hydrochloride (EDC) and N-hydroxysulfosuccinimide (Sulfo-NHS) activated nanoparticles solution, allowed to react using a rotary shaker at room temperature for 4 h, and stored at 4 °C overnight. 1 M glycine and 10 mM Tris (pH 7.5) were added to quench the excess hydroxylamine. The solution was centrifuged at 12,000 rpm for 20 min to remove any unbound peptide and collect the precipitate. Finally, the synthetic peptide-nanoparticles hybrids, GNP-CK-CopA3, were resuspended in PBS and stored at 4 °C for further study.

Characterisation of GNP-CK-CopA3

The characterisation of GNP-CK-CopA3 was determined by various instrumental techniques as previously reported [29], including ultraviolet-visible (UV–Vis), high resolution transmission electron microscopy (HR-TEM), elemental mapping, X-ray diffraction (XRD), selected area diffraction (SAED), energy-dispersive X-ray (EDX), dynamic light scattering (DLS), photoluminescence (PL) [30], and fourier-transform infra-red (FTIR).

Cell lines and culture conditions

Normal human dermal fibroblast cells (NHDFs), human keratinocytes (HaCaTs), and murine macrophage cells (RAW264.7), were obtained from the American Type Culture Collection (ATCC, Manassas, VA, USA) or Korean Cell Line Bank (KCLB, Seoul, Korea). The NHDFs, HaCaTs, and RAW264.7 cells were routinely cultured in complete DMEM containing 10% heat-inactivated FBS and 1% penicillin-streptomycin. The culture conditions were 37 °C in a 5% CO_2 humidified incubator.

Cell viability assay

NHDFs, HaCaTs, and RAW264.7 cells were separately seeded in 96-well plates at a density of 1×104 cells/well and incubated for 24 h to allow attachment. *In vitro* cytotoxicity was analysed after treatment with or without GNP-CK-CopA3 at the indicated concentrations. After 24 h, 100 μL MTT (0.5 mg/mL) was added, and cells were incubated for another 3 h. Then formazan crystals were dissolved in 100 μL DMSO and the optical density was measured at 570 nm by a microplate reader (Molecular Devices Filter Max F5; San Francisco, CA, USA).

Enhanced dark-field (EDF) microscopy

RAW264.7 cells were seeded and grew on 22-mm coverslips in 6-well plates for 24 h and then were incubated with GNP-CK-CopA3 (40 μg/mL) for 3 h. After rinsing with PBS twice, cells were fixed with 4% paraformaldehyde, prepared as slides, and sealed by clear fingernail polish, and finally observed (100×) in a high-resolution illumination microscopy system (Cytoviva Inc., Auburn, AL, USA).

Transmission electron microscopy (TEM)

RAW264.7 cells were seeded in 6-well plates for 24 h and treated with 20 or 40 μg/mL of GNP-CK-CopA3 for 3 h. According to the previously reported [31], collected cell pellets were fixed with 2.5% glutaraldehyde at 4 °C for 8 h, post-fixed with 1% osmium tetroxide for 2 h, and gradually dehydrated with 50, 70, 90, and 100% ethanol for 15 min each. Samples were then embedded in Epon (Sigma-Aldrich). Ultrathin sections (70 nm) were cut in a Leica EM ultramicrotome (Wetzlar, Germany) and put on Cu grids. The sections were finally captured on JEM-1010 TEM (Joel, Tokyo, Japan) operated at 80 kV.

Staining of Lyso-Tracker

RAW264.7 cells grown on the 22-mm coverslips in 6-well plates were treated with GNP-CK-CopA3 for 6 h. After incubation, cells were gently washed with PBS and then 1 ml pre-warmed medium containing 50 nM LysoTracker™ Green DND-26 (Invitrogen, Ltd., Paisley, UK, Ex/Em 504/511 nm) were added. Following a 30 min incubation, the cells were observed by a Leica DM IRB inverted fluorescence microscope with green excitation as the fluorescence filter.

Nitric oxide (NO) assay

RAW264.7 cells grown in 96-well plates were pre-treated with GNP-CK-CopA3 (10–100 μg/mL) for 1 h and followed by adding LPS (1 μg/mL) for 24 h. 100 μL culture supernatant was reacted with 100 μL Griess reagent, and the absorbance was measured at 570 nm by a microplate reader.

Intracellular reactive oxygen species (ROS) production

Cells were treated with GNP-CK-CopA3 (20 and 40 μg/mL) for 1 h prior to exposure with LPS (1 μg/mL) for 24 h. LPS-induced intracellular ROS release was detected according to a Cellular ROS/Superoxide Detection Assay Kit (Cambridge, MA, USA, Ex/Em 490/525 nm). Fluorescence was measured using an LSM 510 and 510 META laser scanning microscope.

Reverse transcription-polymerase chain reaction (RT-PCR)

Cells were pre-treated with GNP-CK-CopA3 for 1 h and then treated with LPS (1 μg/mL) for another 6 h. Total RNA was prepared by a Trizol reagent kit (Invitrogen, Carlsbad, CA,

Table 1. List of primers sequences used in this study.

Gene name	Forward	Reverse
GAPDH	5′-TGAAGGTCGGTGTGAACGGATTTTGGC-3′	5′-TGGTTCACACCCATCACAAACATGG-3′
iNOS	5′-AATGGCAACATCAGGTCGGCCATCACT-3′	5′-GCTGTGTGTCACAGAAGTCTCGAACTC-3′
COX-2	5′-TGCTGGTGGAAAAACCTCGT-3′	5′-AAAACCCACTTCGCCTCCAA-3′
TNF-α	5′-AGCCCACGTCGTAGCAAACCACCAA-3′	5′-AACACCCATTCCCTTCACAGAGCAAT-3′
IL-1β	5′-TGCAGAGTTCCCCAACTGGTACATC-3′	5′-GTGCTGCCTAATGTCCCCTTGAATC-3′
IL-6	5′-GTTCTCTGGGAAATCGTGGA-3′	5′-TGTACTCCAGGTAGCTATGG-3′

USA). The AccuPower RT PreMix Kit and AccuPower HotStar PCR PreMix Kit (Bioneer, Daejeon, Korea) were performed for RT-PCR following the previously published [29]. Sequences for all primers are provided in Table 1.

Western blot analyses

Cells were pre-treated with GNP-CK-CopA3 for 1 h and then treated with LPS (1 μg/mL) for another 2 or 4 h. The protein was extracted using Pierce™ RIPA Buffer (Thermo Scientific, Rockford, USA) and quantified using Protein Assay Dye Reagent Concentrate (Bio-Rad, CA, USA). The total proteins (50 μg) were separated by 10% SDS-PAGE and transferred to PVDF membranes using Protein Gel Electrophoresis Chamber System and iBlot 2 Dry Blotting System (Thermo Fisher Scientific). The membranes were blocked by 5% skim milk at room temperature for 1 h followed by incubation with primary antibodies overnight at 4 °C. After that, the membranes were conjugated with the appropriate horseradish peroxidase-linked secondary antibodies (Santa Cruz, CA, USA) at room temperature for 1 h. The bands were detected with the West-Q Pico ECL Solution (GenDEPOT, Barker, USA) and quantified using ImageJ software.

Immunofluorescence staining

The effect of GNP-CK-CopA3 nuclear translocation of NF-kB p65 was examined by immunofluorescence assay. Cells were fixed in 4% paraformaldehyde and permeabilized with 0.1% Triton X-100 in PBS, and blocked with 2% BSA for 1 h at 37°C. The anti-NF-κB p65 (1:1000) antibody was applied for 1 h followed by a 30 min incubation with fluorescein isothiocyanate (FITC)-conjugated donkey anti-rabbit IgG. After washing in PBS, nuclei were stained with Hoechst 33258, and fluorescence was captured (400× magnification) using a Leica DM IRB inverted fluorescence microscope and quantified using ImageJ software. The nuclei-positively stained cells were counted from five random fields in each well.

Statistical analysis

All data are presented as the mean ± standard error (SEM). Statistical analyses were performed using GraphPad Prism 6 (San Diego, CA, USA). Statistical significance was evaluated by one-way analysis of variance ANOVA with Dunnett's test. be "$p < .05$ were considered statistical significance", and $p < .05$, $p < .01$, and $p < .001$ were described in the figure legends (e.g. $*p < .05$, $**p < .01$, $***p < .001$ or $\#p < .05$, $\#\#p < .01$, $\#\#\#p < .001$).

Results

Characterisation of GNP-CK-CopA3

Gluconacetobacter liquefaciens kh-1 was identified as *Gluconacetobacter liquefaciens* IFO 12388 with high similarity (98%) and G + C mole% content (39.70 mol%) of the genomic DNA have been well characterised previously (Supplementary Figure S1). The biosynthetic GNP-CK-CopA3 was confirmed using a UV–Vis spectral analysis showing significant absorbance at 550 nm (Figure 1(A)). TEM images indicated that the nanoparticles were spherical-shaped with a diameter of 10–30 nm (Figure 1(B)). Meanwhile, these nanoparticles displayed polycrystalline orientation, and the lattice fringes with *d*-spacing of 0.23 nm corresponded to the (111) lattice plane of gold (Figure 1(C)). The distributions of gold elements were clearly visible in the elemental mapping images (Figure 1(D,E)), and the characteristic peak of metallic gold at 2.3 keV was determined by EDX spectroscopy (Figure 1(H)). XRD and SAED analyses showed four major diffraction peaks at 2θ values of 38.18°, 44.40°, 64.56°, and 77.55°, which correspond respectively to the (111), (200), (220), and (311) lattice planes of Bragg's reflection (Figure 1(F,G)). The photoluminescence (PL) spectrum showed the intensity of GNP-CK-CopA3 at 500 nm (Figure 1(I)).

Structural analysis by FTIR spectroscopy

FTIR spectra of GNP-CK-CopA3 (Figure 1(J)), CK (Figure 1(K)), and gold salt (Figure 1(L)), and tabulated of their absorption peaks (Figure 1(M)) are showed in Figure 2. The bands at 3416 and 3386 cm^{-1} characterised as hydroxyl group (O–H) of phenolic compounds structures; at 2960–2876 cm^{-1} caused by C–H stretching vibration of methyl or methylene; at 1655–1542 cm^{-1} represented carbonyl (C=O) and amine (N–H) stretching of amide; at 1453–1311 cm^{-1} represented the CH_3, CH_2 asymmetric deformations; at 1261–1027 cm^{-1} represented the aliphatic ether (C–O) bands; and at 668–562 cm^{-1} represented the =CH in aromatic compounds. We suspect that those peaks result from, on the one hand, the physical interactions (electrostatic, hydrophobic, and affinity interactions) between the ginsenoside CK and GNPs. On the other hand, the peptide CopA3 was covalently linked to GNPs via the coupling of the peptide with amine groups to the carboxylic-group-functionalised of GNPs.

Uptake and intracellular localisation of GNP-CK-CopA3

Cellular uptake of GNP-CK-CopA3 in RAW264.7 macrophages was detected using bright-field and enhanced dark-field (EDF) microscopy (Figure 2(A)). After 3 h incubation, GNP-CK-CopA3 appeared to be uptake by macrophages, as indicated

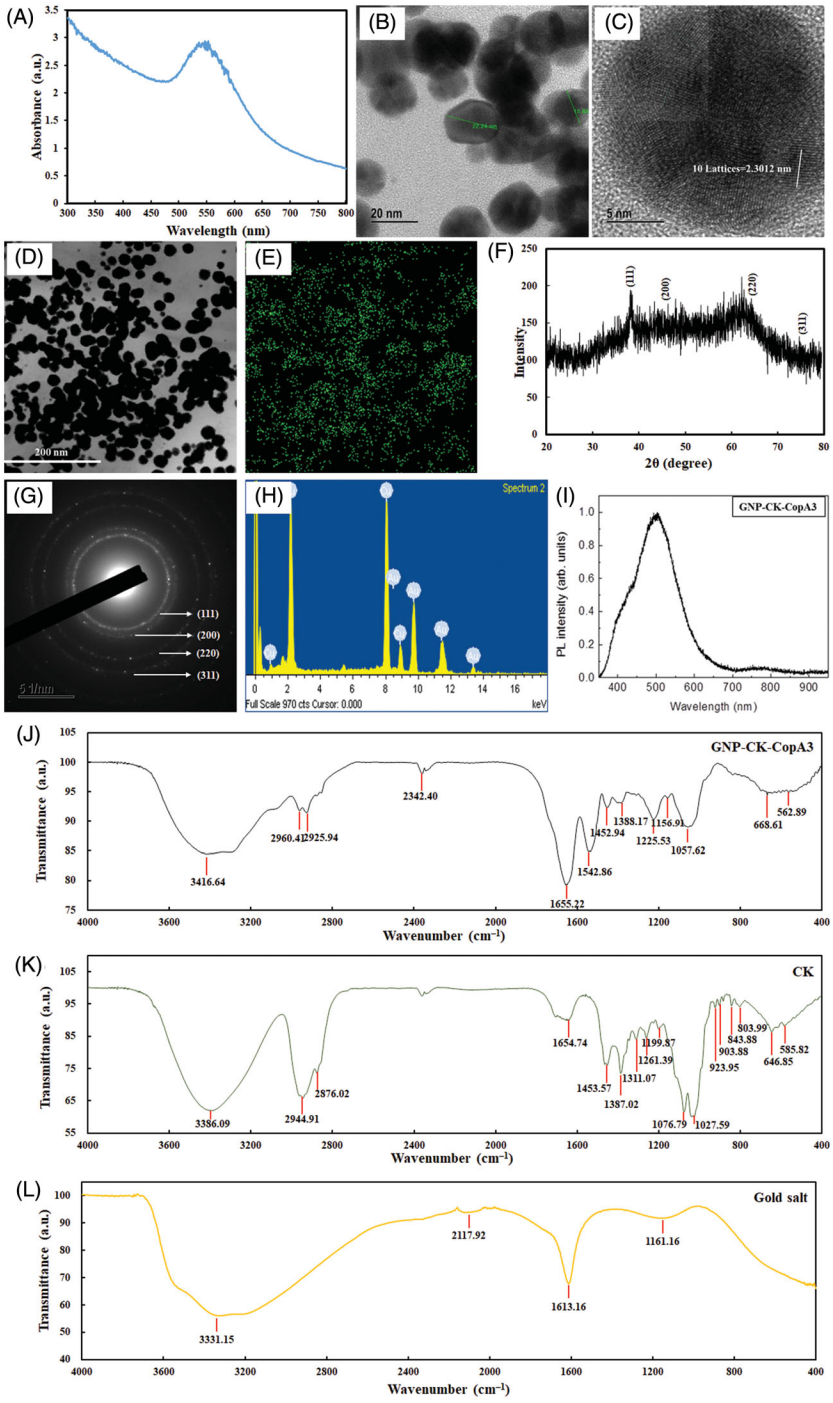

(M)

Type of bond	Wavenumbers (cm^{-1})		
	GNP-CK-CopA3	CK	Gold salt
O-H stretch	3416.64	3386.09	3331.15
C-H stretch	2960.41, 2925.94	2944.91, 2876.02	
C=O of amide	1655.22	1654.74	1613.16
N–H of amide	1542.86		
CH_3, CH_2 asymmetric deformation	1452.94, 1388.17	1453.57, 1387.02, 1311.07	
C-O stretch	1225.53, 1156.51, 1057.62	1261.39, 1199.87, 1076.79, 1027.59	1161.16
=CH of aromatic	668.61, 562.89	646.85, 585.82	

Figure 1. Characterisation of GNP-CK-CopA3. (A) UV–vis absorption spectra, (B) TEM image, (C) HRTEM image, (D and E) Elemental mapping, (F) XRD pattern, (G) SAED pattern, (H) EDX spectrum, and (I) PL of the prepared nanoparticles. FTIR spectra of (J) GNP-CK-CopA3, (K) ginsenoside CK, (L) gold salt, and (M) a tabular view of the functional group profile.

in the aggregated bright white spots. Subsequently, intracellular localisation of GNP-CK-CopA3 was further observed using TEM images (Figure 2(B)). GNP-CK-CopA3 were detected on the membrane and membrane-bound organelles such as endosomes, lysosomes, and large endosomal-vacuoles in RAW264.7 cells. Furthermore, we examined the

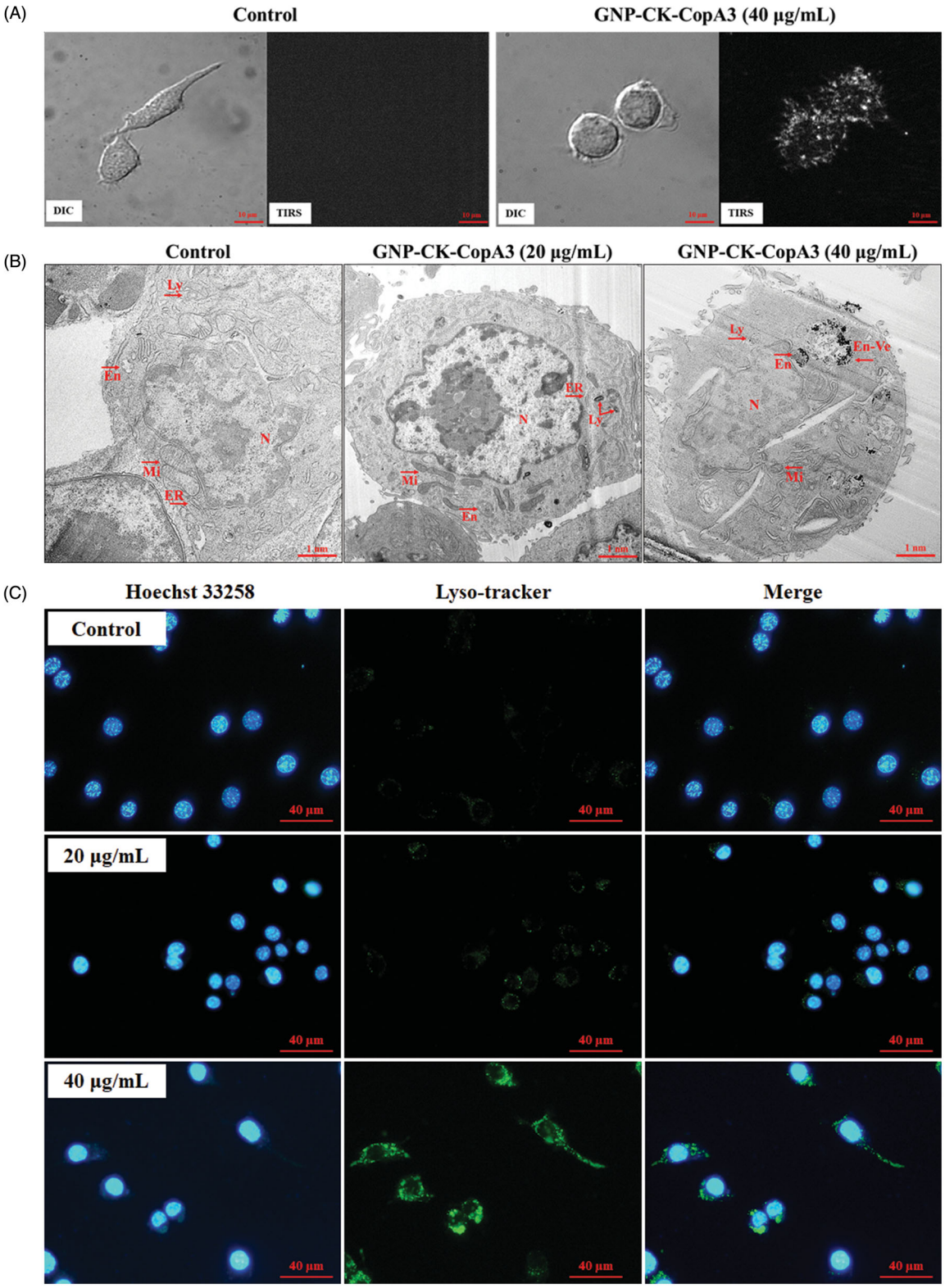

Figure 2. Cellular uptake and localisation of GNP-CK-CopA3. (A) EDF images of RAW264.7 cells after incubation with 40 μg/mL GNP-CK-CopA3 for 3 h. (B) TEM images of RAW264.7 cells after 2 h treatment of 20 and 40 μg/mL GNP-CK-CopA3. (C) Staining analysis for detection of the lysosome (green) and nucleus (blue) in RAW264.7 cells by Lyso-Tracker and Hoechst 33258 staining. All treatments were performed three times ($n = 3$).

fluorescence responses of LysoTracker green after treating with GNP-CK-CopA3 for 6 h in RAW264.7 cells. Hoechst 33258 nucleic acid stain was used for staining the nucleus. In GNP-CK-CopA3-treated cells, lysosomes were visible as specific foci (Figure 2(C)), indicating that GNP-CK-CopA3 disrupts lysosomes in macrophages.

Cytotoxicity of GNP-CK-CopA3

The cytotoxicity of GNP-CK-CopA3 was investigated using the MTT assay in the NHDFs, HaCaTs, and RAW264.7 cells. In NHDFs (Figure 3(A)), no toxicity was noticed from 2.5 to 80 μg/mL GNP-CK-CopA3, in HaCaTs, a small inhibitory effect

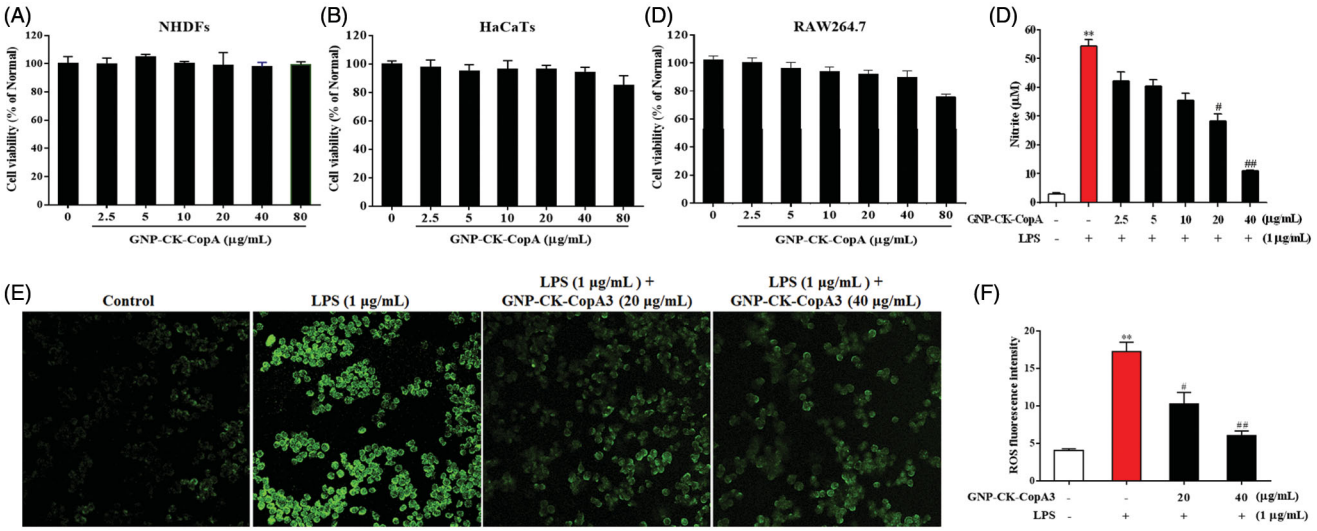

Figure 3. Effect of GNP-CK-CopA3 on cell viability and NO and intracellular ROS production in LPS-stimulated RAW264.7 cells. Cell viability of (A) NHDFs, (B) HaCaTs, and (C) Cells incubation with different concentrations of GNP-CK-CopA3 for 24 h was determined by MTT assay. (D) NO production induced by 1 μg/mL LPS with or without GNP-CK-CopA3 was assessed in RAW264.7 cells. (E) Cells were stained with cellular ROS/Superoxide Detection Assay Kit and observed in fluorescence microscopy with 200× magnification. (F) Statistical analysis of the mean fluorescence intensity of ROS staining. Data are presented as mean ± SEM. $^{*}p < .05$ and $^{**}p < .01$ vs. normal control group; $\#p < .05$ and $\#\#p < .01$ vs. LPS-treated group. All treatments were performed three times ($n = 3$).

was noticed at 80 μg/mL, indicating that HaCaTs was more sensitive (Figure 3(B)) than NHDFs. However, it is clear that 80 μg/mL GNP-CK-CopA3 caused toxicity (31.9% death) to the RAW264.7 cells (Figure 3(C)). As a control, the cytotoxicity of CopA3 was investigated using the MTT assay in RAW264.7 cells (Supplementary Figure S2), and also the cell cannot survive under same concentration of CK.

Effects of GNP-CK-CopA3 on NO production

The NO secretion in LPS-activated macrophages was indirectly estimated by nitrite determination. As shown in Figure 3(D), pre-treatment with GNP-CK-CopA3 (20 and 40 μg/mL) significantly inhibited the LPS-induced (1 μg/mL) nitrate levels in macrophages without cytotoxicity (Figure 3(C)).

ROS production

It has been reported that ROS are essential for LPS-induced inflammation.[32] ROS secretion was elevated by 76.6% after LPS treatment (Figure 3(E,F)). However, pre-treatment with 20 and 40 μg/mL GNP-CK-CopA3 effectively inhibited ROS production by 40.4 and 65.05%, respectively.

mRNA and protein expression of pro-inflammatory factors

The excessive production of pro-inflammatory mediators and cytokines, such as inducible nitric oxide synthase (iNOS), cyclooxygenase-2 (COX-2), tumour necrosis factor-α (TNF-α), interleukin (IL)-1β, and IL-6, by macrophages, can cause various chronic inflammatory diseases [33]. Therefore, we investigated whether GNP-CK-CopA3 affected the gene and protein expression of those factors. Macrophages were pre-treated with GNP-CK-CopA3 (20 or 40 μg/mL) for 1 h and then irritated by LPS (1 μg/mL) for 24 h. LPS led to the increase of mRNA iNOS, COX-2, TNF-α, IL-1β, and IL-6 expression by 84.0, 59.7, 63.4, 54.4, and 80.0%, respectively, compared with untreated cells (Figure 4(A)). However, cells pre-treated with GNP-CK-CopA3 (40 μg/mL) showed significant decrease by 34.7, 51.9, 24.7, 33.6, and 37.0%, respectively, compared with the LPS stimulated cells. Furthermore, the LPS-induced up-regulation of protein expression of iNOS, COX-2, TNF-α, IL-1β, and IL-6 was also inhibited by 44.8, 32.0, 39.3, 58.5, and 58.9%, through blocking of IL-1β post translation processing, when pre-treated with 40 μg/mL GNP-CK-CopA3 (Figure 4(B)).

Effects of GNP-CK-CopA3 on the NF-κB signalling pathway

In macrophages, various intracellular signalling pathways, such as the nuclear factor kappa B (NF-κB) pathway, have been found to be highly associated with the anti-inflammatory action of GNPs [34]. Herein, RAW264.7 cells were pre-treated with GNP-CK-CopA3 (20 or 40 μg/mL) for 1 h and then irritated by LPS (1 μg/mL) for 2 h [35]. In LPS-activated inflammatory condition, inhibitor kappa B-alpha (IκBα) was phosphorylated and ubiquitinated, leading to the nuclear translocation of NF-κB from the cytoplasm (Figure 5(A–E)), whereas pre-treatment with the nanoparticles efficiently inhibited the protein IκBα phosphorylation and degradation. Additionally, nuclear NF-κB p65 subunit protein expression was also inhibited by pre-treatment GNP-CK-CopA3, indicating the nuclear transcription of NF-κB was suppressed in LPS-irritated RAW264.7 cells.

By immunofluorescence staining, we further examined whether GNP-CK-CopA3 inhibits the activation of NF-κB in RAW264.7 cells. As expected, LPS stimulation induced translocation and accumulation of NF-κB p65 from the cytoplasm

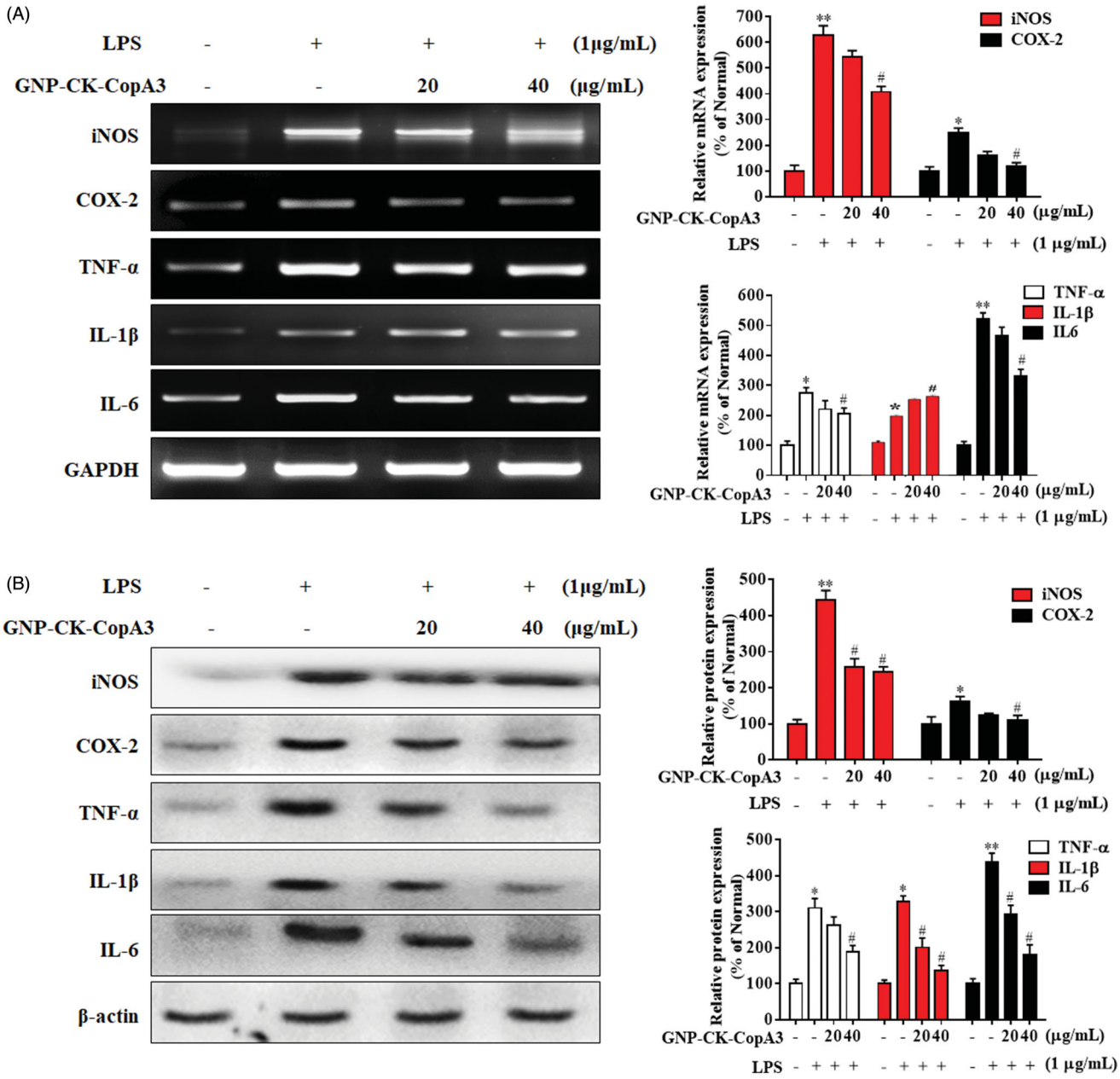

Figure 4. Effect of GNP-CK-CopA3 on pro-inflammatory cytokines iNOs, COX-2, TNF-α, IL-1β, and IL-6 expression in LPS-induced RAW264.7 cells. (A) The mRNA expression was quantified by RT-PCR. (B) The protein expression was determined by Western blotting. The densitometric quantification was done by ImageJ software. GAPDH and β-actin were used as internal control for RT-PCR and Western blotting, respectively. Data are presented as mean ± SEM. $^{*}p < 0.05$ and $^{**}p < 0.01$ vs. normal control group; $\#p < 0.05$ vs. LPS-treated group. All treatments were performed three times ($n = 3$).

to the nucleus, however, it was dramatically inhibited in GNP-CK-CopA3 (Figure 5(F))

Effects of GNP-CK-CopA3 on the MAPK signalling pathway

The mitogen-activating protein kinases (MAPKs) are one of the key transcription factors in regulating inflammation-specific genes. The phosphorylation of extracellular signal-regulated kinase (ERK) and p38 MAPK significantly increased after LPS treatment, but pre-treatment with GNP-CK-CopA3 (20 or 40 μg/mL) for 1 h dramatically attenuated the LPS-induced phosphorylation (Figure 6). Meanwhile, the total expression levels of ERK and p38 did not differ significantly among the groups.

Discussion

Recently, GNPs have been used to deliver drugs for cancer therapies and immune-regulation, such as 5-fluorouracil [36], doxorubicin [37], and curcumin [7]. In our previous report, we used *Lactobacillus kimchicus* DCY51^{T} to synthesise GNPs for the delivery of ginsenoside CK. The CK-loaded GNP was confirmed as an effective photothermal therapy agent with synergistic chemotherapeutic effects for the treatment of cancer [38]. Additionally, to improve the stability and

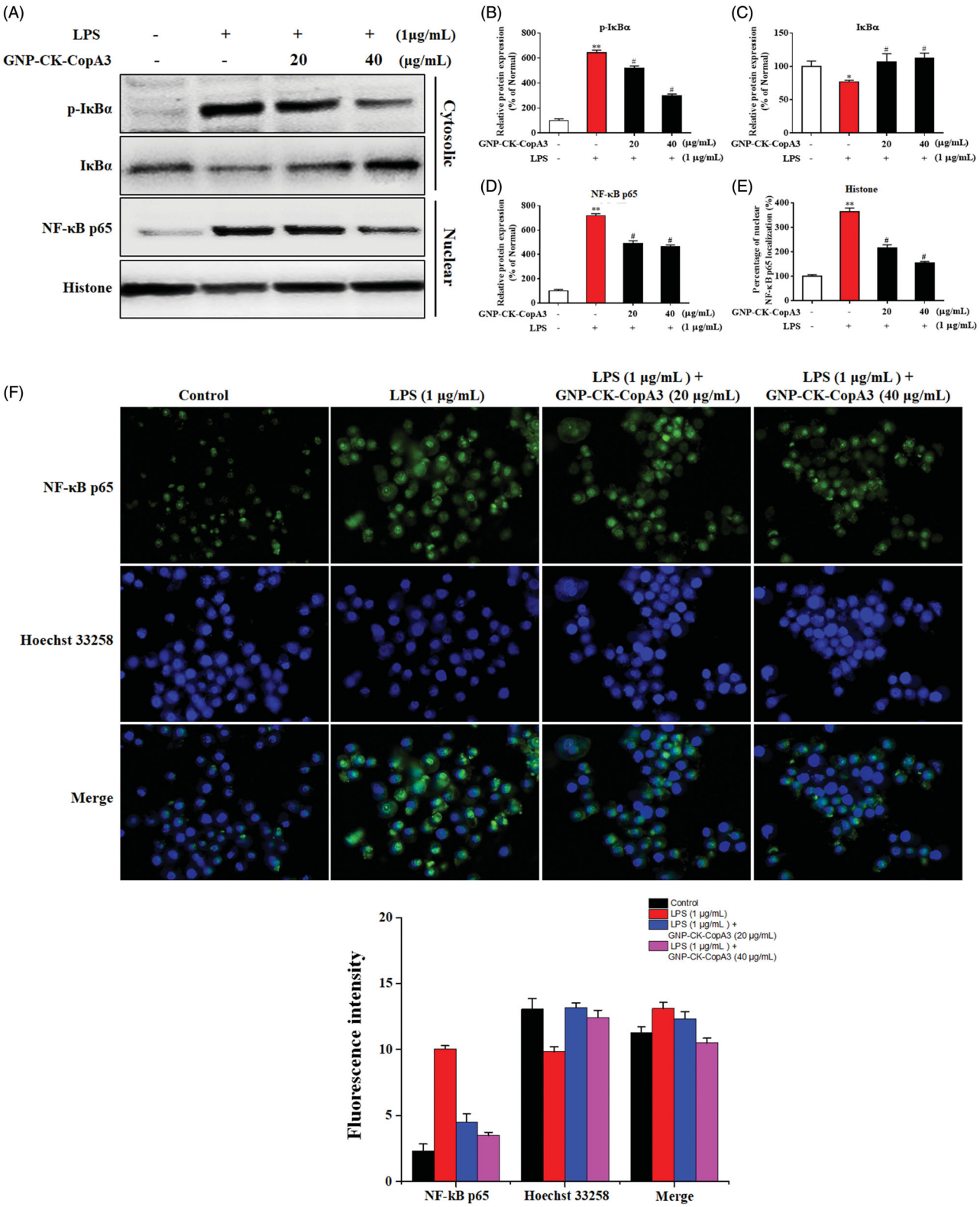

Figure 5. Effect of GNP-CK-CopA3 on LPS-induced NF-κB activation. (A) RAW264.7 cells were treated with GNP-CK-CopA3 for 1 h prior to LPS (1 μg/mL) for 4 h. The protein expression of p-IκBα, IκBα in the cytoplasm and NF-κB p65 in the nucleus were determined by Western blotting. The relative density of (B) p-IκBα, (C) IκBα, (D) NF-κB p65 and (E) Histone. (F) NF-kB nuclear translocation was assessed by immunofluorescence staining for NF-kB p65 antibody (green) and the nuclei were detected by Hoechst (blue). The p65 nuclei-positively stained cells were quantified as the percentage of control group. Densitometric analysis was done by ImageJ software. Data are presented as mean ± SEM. $^{*}p < .05$ and $^{**}p < .01$ vs. normal control group; $^{\#}p < .05$ vs. LPS-treated group. All treatments were performed three times ($n = 3$).

function of the CK-loaded GNPs, we conjugated with the peptide CopA3. The CopA3 is a 9-mer peptide (LLCIALRKK-NH_2) derived from coprisin [39]. Its amino acid residues were used to covalent coupling to the carboxylic-group-functionalised GNPs [17]. Yang et al. [40] suggested that peptide-capped GNPs achieved more cellular internalisation and

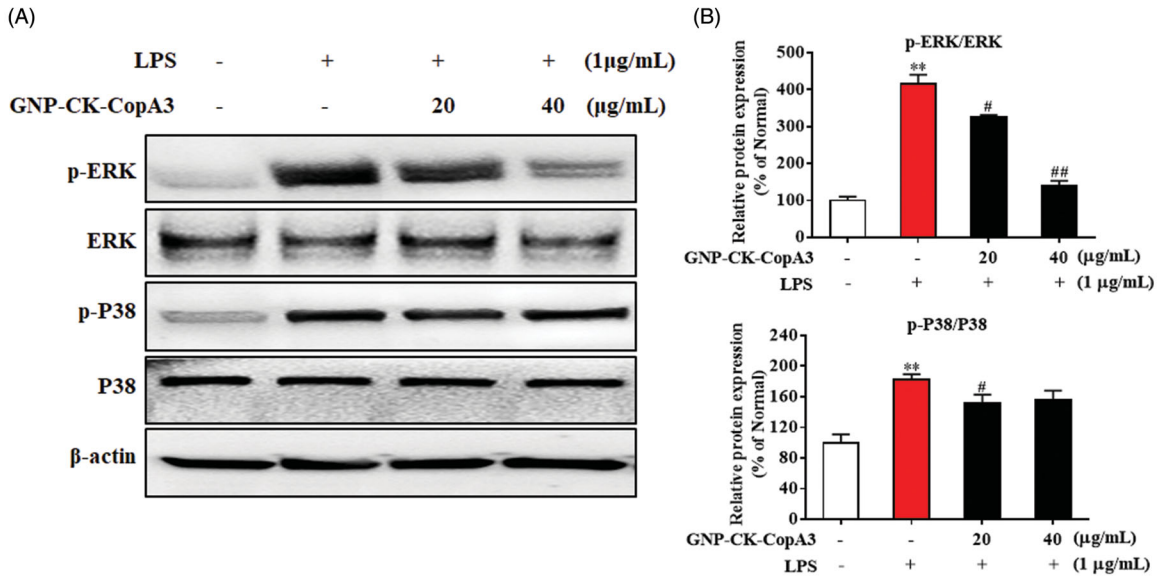

Figure 6. Effect of GNP-CK-CopA3 on LPS-induced MAPK activation. (A) After the treatment of LPS (1 μg/mL) for 2 h with or without GNP-CK-CopA3, the protein expression levels of p-ERK and p-p38 were measured by Western blotting. (B) Densitometric analysis was done by ImageJ software. Data are presented as mean ± SEM. $^{**}p < .01$ vs. normal control group; $\#p < .05$ and $\#\#p < .01$ vs. LPS-treated group. All treatments were performed three times ($n = 3$).

prolonged intracellular retention compared with citrate-capped GNPs because of their positive surface charges. GNP-CK-CopA3 nanoparticles was smaller in size and were accumulated intracellularly by endocytosis. And it endured by EDF, TEM, and Lyso-Tracker images indicated that GNP-CK-CopA3 were trapped as clusters in either endosomes or lysosomes in RAW264.7 cells. CK has excellent physiological activity but it also showes cytotoxicity. Synthesised GNP-CK-CopA3 contain a small amount of CK (lower than 10 ppm), which may lower cytotoxicity with good permeability effect in to Raw264.7 cells. Peptide conugated GNP-CK-CopA3 can be suggested for reducing the cytotoxicity of drug, inducing more biological activity, and increasing durg absorption into the target cells.

Macrophages are the primary contributors to the initiation of potentially pathological inflammation and the progression of autoimmune and auto-inflammatory diseases including cancer, rheumatoid arthritis, cardiovascular disease, atherosclerosis, and Alzheimer's disease [41]. In the early phase of a disease, the innate immune system and Toll-like receptor (TLR) signalling can recognise and respond to diverse microbial epitope pathogen-associated molecular patterns such as LPS [42]. However, excessive TLR responses cause many acute and chronic human inflammatory diseases and cancers. Activated TLR4 elicits the production of pro-inflammatory mediators and cytokines, including NO, iNOS, COX-2, TNF-α, IL-1β, and IL-6. During cellular metabolism, the overproduction of ROS can also contribute to the development of cancer, aging, and inflammation [32]. Zhu *et al.* reported that GNPs significantly attenuated the rise in ROS/RNS-mediated inflammatory responses [43]. Similar to the previous findings, our preliminary study also indicated that CopA3 inhibited the NO production in LPS-stimulated RAW264.7 cells (Supplementary Figure 2A) [27]. Therefore, in our study, the effective inhibition of GNP-CK-CopA3 in LPS-induced production of NO and overexpression of mRNA and protein of pro-inflammatory cytokines was probably due to the combined role of both CopA3 and nanoparticles.

Studies have suggested that both NF-κB and MAPK signalling activation are responsible for the initiation and progression of LPS-induced inflammation [44]. Ginsenoside CK has been widely studied the immunopharmacological activities both *in vivo* and *in vitro*. It was confirmed to regulate inflammation through inhibition of systemic inflammatory cytokines production, MAPKs activation [45], and NF-κB activation [46]. Dysregulated NF-κB is accompanied by the ubiquitination and degradation of IκBα, and the nucleus translocation of activated NF-κB subunits, which ultimately leads to the induction of pro-inflammatory cytokines [47]. In our study, GNP-CK-CopA3 showed anti-inflammatory action by suppressing the protein IκBα phosphorylation and NF-κB nuclear translocation in LPS-activated RAW264.7 cells.

Oxidative stress and ROS are also the causative factors of various inflammatory diseases. Overproduction of ROS induced the phosphorylation of three MAPKs, including JNK, ERK, and p38 [48]. Manna et al. [49] reported that pomegranate peel extract-stabilized GNPs reduced the pro-inflammatory burden by modulating the MAPK and NF-κB pathways. In the current study, the phosphorylated form of ERK and p38 was decreased by GNP-CK-CopA3 in LPS-stimulated RAW264.7 macrophages. It seems unclear that GNP-CK-CopA3 has an anti-inflammatory effect through directly inhibiting NF-kB-signalling pathway or through neutralising LPS, since CopA3 is an AMP. Compared to CopA3, GNP-CK-CopA3 showed more significant anti-inflammatory effect towards RAW264.7 cells, can be suggested for reducing cytotoxicity of drug, inducing more biological activity, and increasing drug absorption into the target cells. Whether or not direct interaction of GCk-CopA3 with LPS may thus have profound impact on antiimflamatory signalling events.

Conclusions

Overall, we synthesised GNPs using *Gluconacetobacter liquefaciens* kh-1 for loading ginsenoside CK and conjugating peptide CopA3. GNP-CK-CopA3 could inhibit both NF-κB and MAPKs activation thereby inhibiting the production of pro-inflammatory cytokines in LPS-stimulated macrophages *in vitro*. This study provides foundational data for the investigation of anti-inflammatory approaches of the peptide-GNP hybrids *in vivo* animal models and is underway.

Disclosure statement

No potential conflict of interest was reported by the author(s).

Author contributions

YL wrote the main manuscript; HP revised the manuscript; SHK prepared gold nanoparticle; JSH and SCK supplied the insect peptide CopA3 and *Gluconacetobacter liquefaciens*, respectively; CHK, THY provided the foundation support; YJK made the overall experiment design and discussion. All authors reviewed and approved the final manuscript.

Funding

This work was carried out with support of the "Cooperative Research Program for Agriculture Science and Technology Development (Project No. PJ0128132019 & PJ01325601)" Rural Development Administration grant, and also supported by a grant from the Basic Science Research Programme through the National Research Foundation of Korea funded by the Ministry of Education [2019R1A2C1010428], Republic of Korea.

References

[1] Kim JH. Pharmacological and medical applications of Panax ginseng and ginsenosides: a review for use in cardiovascular diseases. J Ginseng Res. 2018;42(3):264–269.
[2] Guo M, Xiao J, Sheng X, et al. Ginsenoside Rg3 mitigates atherosclerosis progression in diabetic apoE–/– mice by skewing macrophages to the M2 phenotype. Front Pharmacol. 2018;9:464.
[3] Riaz M, Rahman NUr, Zia-Ul-Haq M, et al. Ginseng: a dietary supplement as immune-modulator in various diseases. Trends Food Sci Technol. 2019;83:12–30.
[4] Nguyen NH, Nguyen CT. Pharmacological effects of ginseng on infectious diseases. Inflammopharmacol. 2019;27(5):871–883.
[5] Zhang J, Wang Y, Jiang Y, et al. Enhanced cytotoxic and apoptotic potential in hepatic carcinoma cells of chitosan nanoparticles loaded with ginsenoside compound K. Carbohydr Polym. 2018; 198:537–545.
[6] Lu S, Luo Y, Zhou P, et al. Ginsenoside compound K protects human umbilical vein endothelial cells against oxidized low-density lipoprotein-induced injury via inhibition of nuclear factor-kappaB, p38, and JNK MAPK pathways. J Ginseng Res. 2019;43(1): 95–104.
[7] Wong KE, Ngai SC, Chan KG, et al. Curcumin nanoformulations for colorectal cancer: a review. Front Pharmacol. 2019;10:152.
[8] Lopez-Chaves C, Soto-Alvaredo J, Montes-Bayon M, et al. Gold nanoparticles: distribution, bioaccumulation and toxicity. *In vitro* and *in vivo* studies. Nanomed Nanotechnol Biol Med. 2018;14(1): 1–12.
[9] Li X, Huang Q, Wang M, et al. Compound K inhibits autophagy-mediated apoptosis through activation of the PI3K-Akt signaling pathway thus protecting against ischemia/reperfusion injury. Cell Physiol Biochem. 2018;47(6):2589–2601.
[10] Lee J-O, Choi E, Shin KK, et al. Compound K, a ginsenoside metabolite, plays an antiinflammatory role in macrophages by targeting the AKT1-mediated signaling pathway. J Ginseng Res. 2019;43(1):154–160.
[11] Park J-S, Shin JA, Jung J-S, et al. Anti-inflammatory mechanism of compound K in activated microglia and its neuroprotective effect on experimental stroke in mice. J Pharmacol Exp Ther. 2012; 341(1):59–67.
[12] Herizchi R, Abbasi E, Milani M, et al. Current methods for synthesis of gold nanoparticles. Artif Cells Nanomed Biotechnol. 2016; 44(2):596–602.
[13] Pérez ZEJ, Mathiyalagan R, Markus J, et al. Ginseng-berry-mediated gold and silver nanoparticle synthesis and evaluation of their *in vitro* antioxidant, antimicrobial, and cytotoxicity effects on human dermal fibroblast and murine melanoma skin cell lines. IJN. 2017;12:709–723.
[14] Ahmed S, Ikram S. Biosynthesis of gold nanoparticles: a green approach. J Photochem Photobiol B Biol. 2016;161:141–153.
[15] Kikuchi F, Kato Y, Furihata K, et al. Formation of gold nanoparticles by glycolipids of *Lactobacillus casei*. Sci Rep. 2016;6(1): 34626.
[16] Markus J, Mathiyalagan R, Kim Y-J, et al. Intracellular synthesis of gold nanoparticles with antioxidant activity by probiotic *Lactobacillus kimchicus* DCY51T isolated from Korean kimchi. Enzyme Microb Technol. 2016;95:85–93.
[17] Matea CT, Mocan T, Tabaran F, et al. Rational design of gold nanocarrier for the delivery of JAG-1 peptide. J Nanobiotechnol. 2015;13(1):41.
[18] Li XY, Feng FY, Zhou XD, et al. Rational design of an anchoring peptide for high-efficiency and quantitative modification of peptides and DNA strands on gold nanoparticles. Nanoscale. 2018; 10(24):11491–11497.
[19] Liu JY, Peng QA. Protein-gold nanoparticle interactions and their possible impact on biomedical applications. Acta Biomater. 2017; 55:13–27.
[20] Yang H, Fung SY, Xu S, et al. Amino acid-dependent attenuation of toll-like receptor signaling by peptide-gold nanoparticle hybrids. ACS Nano. 2015;9(7):6774–6784.
[21] Deng J, Yao MY, Gao CY. Cytotoxicity of gold nanoparticles with different structures and surface-anchored chiral polymers. Acta Biomater. 2017;53:610–618.
[22] Liu L, Xu K, Wang H, et al. Self-assembled cationic peptide nanoparticles as an efficient antimicrobial agent. Nature Nanotech. 2009;4(7):457–463.
[23] Nam ST, Kim DH, Lee MB, et al. Insect peptide CopA3-induced protein degradation of p27Kip1 stimulates proliferation and protects neuronal cells from apoptosis. Biochem Biophys Res Commun. 2013;437(1):35–40.
[24] Kim IW, Kim SJ, Kwon YN, et al. Effects of the synthetic coprisin analog peptide, CopA3 in pathogenic microorganisms and mammalian cancer cells. J Microbiol Biotechnol. 2012;22(1):156–158.
[25] Ha Lee J, Kim I-w, Pyo Shin Y, et al. Enantiomeric CopA3 dimer peptide suppresses cell viability and tumor xenograft growth of human gastric cancer cells. Tumor Biol. 2016;37(3):3237–3245.
[26] Kim DH, Hwang JS, Lee IH, et al. The insect peptide CopA3 increases colonic epithelial cell proliferation and mucosal barrier function to prevent inflammatory responses in the gut. J Biol Chem. 2016;291(7):3209–3223.
[27] Nam HJ, Oh AR, Nam ST, et al. The insect peptide CopA3 inhibits lipopolysaccharide-induced macrophage activation. J Pept Sci. 2012;18(10):650–656.
[28] Lee S, Yu H, Kang SH. Selective fluorescent-free detection of biomolecules on nanobiochips by wavelength dependent-enhanced dark field illumination. Chem Commun. 2013;49(75):8335–8337.
[29] Liu Y, Kim S, Kim YJ, et al. Green synthesis of gold nanoparticles using Euphrasia officinalisleaf extract to inhibit lipopolysaccharide-induced inflammation through NF-κB and JAK/STAT pathways in RAW 264.7 macrophages. IJN. 2019;14:2945–2959.

[30] Kim JM, Kim S, Hwang SW, et al. Strong enhancement of emission efficiency in GaN light-emitting diodes by plasmon-coupled light amplification of graphene. Nanotechnology. 2018;29(5):055201.
[31] Katsumiti A, Tomovska R, Cajaraville MP. Intracellular localization and toxicity of graphene oxide and reduced graphene oxide nanoplatelets to mussel hemocytes *in vitro*. Aquat Toxicol. 2017; 188:138–147.
[32] Bist G, Pun NT, Magar TBT, et al. Inhibition of LPS-stimulated ROS production by fluorinated and hydroxylated chalcones in RAW 264.7 macrophages with structure-activity relationship study. Bioorg Med Chem Lett. 2017;27(5):1205–1209.
[33] Zou Y-H, Zhao L, Xu Y-K, et al. Anti-inflammatory sesquiterpenoids from the traditional Chinese medicine *Salvia plebeia*: regulates pro-inflammatory mediators through inhibition of NF-κB and Erk1/2 signaling pathways in LPS-induced Raw264. 7 cells. J Ethnopharmacol. 2018;210:95–106.
[34] Ni C, Zhou J, Kong N, et al. Gold nanoparticles modulate the crosstalk between macrophages and periodontal ligament cells for periodontitis treatment. Biomaterials. 2019;206:115–132.
[35] Bagaev AV, Garaeva AY, Lebedeva ES, et al. Elevated pre-activation basal level of nuclear NF-kappaB in native macrophages accelerates LPS-induced translocation of cytosolic NF-kappaB into the cell nucleus. Sci Rep. 2019;9(1):4563.
[36] Li J, Wang Y, Liang R, et al. Recent advances in targeted nanoparticles drug delivery to melanoma. Nanomed Nanotechnol Biol Med. 2015;11(3):769–794.
[37] Zhou M, Wei W, Chen X, et al. pH and redox dual responsive carrier-free anticancer drug nanoparticles for targeted delivery and synergistic therapy. Nanomed Nanotechnol Biol Med. 2019;20: 102008.
[38] Kim YJ, Perumalsamy H, Markus J, et al. Development of Lactobacillus kimchicus DCY51(T)-mediated gold nanoparticles for delivery of ginsenoside compound K: *in vitro* photothermal effects and apoptosis detection in cancer cells. Artif Cells Nanomed Biotechnol. 2019;47(1):30–44.
[39] Kang B-R, Kim H, Nam S-H, et al. CopA3 peptide from Copris tripartitus induces apoptosis in human leukemia cells via a caspase-independent pathway. BMB Rep. 2012;45(2):85–90.
[40] Yang C, Uertz J, Yohan D, et al. Peptide modified gold nanoparticles for improved cellular uptake, nuclear transport, and intracellular retention. Nanoscale. 2014;6(20):12026–12033.
[41] Li X, Shen J, Jiang Y, et al. Anti-inflammatory effects of chloranthalactone B in LPS-stimulated RAW264. 7 cells. IJMS. 2016;17(11): 1938.
[42] Yang H, Kozicky L, Saferali A, et al. Endosomal pH modulation by peptide-gold nanoparticle hybrids enables potent anti-inflammatory activity in phagocytic immune cells. Biomaterials. 2016;111: 90–102.
[43] Zhu S, Jiang X, Boudreau MD, et al. Orally administered gold nanoparticles protect against colitis by attenuating Toll-like receptor 4-and reactive oxygen/nitrogen species-mediated inflammatory responses but could induce gut dysbiosis in mice. J Nanobiotechnol. 2018;16(1):86.
[44] Gul A, Kunwar B, Mazhar M, et al. Rutin and rutin-conjugated gold nanoparticles ameliorate collagen-induced arthritis in rats through inhibition of NF-kappaB and iNOS activation. Int Immunopharmacol. 2018;59:310–317.
[45] Cuong TT, Yang C-S, Yuk J-M, et al. Glucocorticoid receptor agonist compound K regulates Dectin-1-dependent inflammatory signaling through inhibition of reactive oxygen species. Life Sci. 2009;85(17–18):625–633.
[46] Park E-K, Shin Y-W, Lee H-U, et al. Inhibitory effect of ginsenoside Rb1 and compound K on NO and prostaglandin E2 biosyntheses of RAW264. 7 cells induced by lipopolysaccharide. Biol Pharm Bull. 2005;28(4):652–656.
[47] de Carvalho TG, Garcia VB, de Araujo AA, et al. Spherical neutral gold nanoparticles improve anti-inflammatory response, oxidative stress and fibrosis in alcohol-methamphetamine-induced liver injury in rats. Int J Pharm. 2018;548(1):1–14.
[48] Jin CH, So YK, Han SN, et al. Isoegomaketone upregulates heme oxygenase-1 in RAW264. 7 cells via ROS/p38 MAPK/Nrf2 pathway. Biomol Therap. 2016;24(5):510–516.
[49] Manna K, Mishra S, Saha M, et al. Amelioration of diabetic nephropathy using pomegranate peel extract-stabilized gold nanoparticles: assessment of NF-κB and Nrf2 signaling system. IJN. 2019; 14:1753–1777.